How to cite: *Angew. Chem. Int. Ed.* **2023**, *62*, e202309779
doi.org/10.1002/anie.202309779

Microgels

Varying the Stiffness and Diffusivity of Rod-Shaped Microgels Independently through Their Molecular Building Blocks

Yonca Kittel, Luis P. B. Guerzoni, Carolina Itzin, Dirk Rommel, Matthias Mork, Céline Bastard, Bernhard Häßel, Abdolrahman Omidinia-Anarkoli, Silvia P. Centeno, Tamás Haraszti, Kyoohyun Kim, Jochen Guck, Alexander J. C. Kuehne, and Laura De Laporte**

Abstract: Microgels are water-swollen, crosslinked polymers that are widely used as colloidal building blocks in scaffold materials for tissue engineering and regenerative medicine. Microgels can be controlled in their stiffness, degree of swelling, and mesh size depending on their polymer architecture, crosslink density, and fabrication method—all of which influence their function and interaction with the environment. Currently, there is a lack of understanding of how the polymer composition influences the internal structure of soft microgels and how this morphology affects specific biomedical applications. In this report, we systematically vary the architecture and molar mass of polyethylene glycol-acrylate (PEG-Ac) precursors, as well as their concentration and combination, to gain insight in the different parameters that affect the internal structure of rod-shaped microgels. We characterize the mechanical properties and diffusivity, as well as the conversion of acrylate groups during photopolymerization, in both bulk hydrogels and microgels produced from the PEG-Ac precursors. Furthermore, we investigate cell-microgel interaction, and we observe improved cell spreading on microgels with more accessible RGD peptide and with a stiffness in a range of 20 kPa to 50 kPa lead to better cell growth.

[*] Y. Kittel, L. P. B. Guerzoni, C. Itzin, D. Rommel, M. Mork, C. Bastard, B. Häßel, A. Omidinia-Anarkoli, S. P. Centeno, T. Haraszti, L. De Laporte
DWI-Leibniz Institute for Interactive Materials e.V.
Forckenbeckstraße 50, 52074 Aachen (Germany)
E-mail: delaporte@dwi.rwth-aachen.de

Y. Kittel, L. P. B. Guerzoni, C. Itzin, D. Rommel, M. Mork, C. Bastard, B. Häßel, A. Omidinia-Anarkoli, T. Haraszti, L. De Laporte
Institute of Technical and Macromolecular Chemistry, RWTH Aachen University
Worringerweg 1–2, 52074 Aachen (Germany)

K. Kim, J. Guck
Max Planck Institute for the Science of Light and Max-Planck-Zentrum für Physik und Medizin
Staudtstraße 2, 91058 Erlangen (Germany)

Y. Kittel, A. J. C. Kuehne
Institute of Organic and Macromolecular Chemistry, Ulm University
Albert-Einstein Allee 11, 89081 Ulm (Germany)
E-mail: alexander.kuehne@uni-ulm.de

C. Bastard, L. De Laporte
Center for Biohybrid Medical Systems (CBMS), Advanced Materials for Biomedicine (AMB), Institute of Applied Medical Engineering (AME)
Forckenbeckstraße 55, 52074 Aachen (Germany)

Introduction

Micron-scaled gels represent powerful colloidal building blocks for scaffold materials in tissue engineering and regenerative medicine. Such microgels are crosslinked polymer networks that are swollen with water. These finite, colloidal gels exhibit variable stiffness, degree of swelling, mesh size, and shape, all of which influence their function and response to their environment and depend on the internal structure of the microgels.[1,2] The term *internal structure* has been coined to account for the fact that heterogeneity in gel networks may occur across length scales, spanning several orders of magnitude. The internal structure depends on the architecture, molar mass, and concentration of the molecular building blocks, as well as the mechanism of crosslinking and its rate.[3–6] The internal structure affects the diffusivity (the diffusion of molecules through the network), the swelling and shrinking capacity of a microgel in response to external triggers, such as pH, light, and temperature, and the mechanical and chemical interaction with their surroundings, for example other microgels, proteins, cells, or plants.[7,8]

In bulk hydrogels, the internal structure has been analysed with regard to its effect on the diffusivity, correlating mesh size and morphology to diffusion properties.[9–14] Many studies have focussed on hydrogels made from polyethylene glycol (PEG), representing a biologically inert and biocompatible polymer, which is clinically approved and currently used in patients as solubilizing units in imaging probes and contrast agents, in many drug

formulations, and as injectable organ spacers.[15–17] The diffusivity of PEG hydrogels depends on the mechanism that is chosen for crosslinking during hydrogel network formation. More specifically, *chain-growth* polymerization produces a different network architecture and internal structure compared to *step-growth* polymerization.[18] Even though step-growth polymerization leads to more homogeneous polymer network structures and controlled degradation rates, and is therefore often used for the incorporation of cells inside hydrogels for tissue engineering application, it is limited by lower polymerization and thus hydrogel production rates compared to chain-growth polymerization.[19] Chain-growth polymerization results in more heterogeneous polymer network structures but enables faster polymerization and, therefore, the production of microgels in high-throughput systems.

In another example, the swelling ratio and internal pore structure of hydrogels formed from poly(*N*-isopropylacrylamide) (NIPAm), copolymerized with PEG-diacrylate (PEG-DA) as a crosslinker, can be precisely tuned by changing the molar mass of the PEG-DA and its compositional ratio (NIPAm to PEG-DA).[20] By contrast, systematic studies to alter the internal structure of micron-scaled PEG-based microgels and its effect on stiffness, swelling behaviour, and diffusivity are absent to date.

Microgels with dimensions in the range of several micrometers are typically produced by employing one of the following fabrication techniques: in-mold polymerization, photo-lithography, stop flow lithography, droplet microfluidics, or compartmentalized jet polymerization.[21–24] In the case of confined microfluidic droplets or in filled cavities, the chosen process of crosslinking and its rate lead to different physical and mechanical properties of the microgels—in turn these vary greatly from bulk hydrogels.[25] For example, in the case of in-mold polymerization, a liquid non-reactive PEG filler has been employed to avoid solvent evaporation during crosslinking.[21] When crosslinking the mixture of pre-polymer in the presence of an inert polymer filler by free radical polymerization, phase separation occurs, which is well described by the Flory-Huggins-theory as the molecular weight increases during polymerization, affecting the Gibbs-free energy. This leads to large mesh sizes and soft microgels. When the microgels are prepared via thermally-induced amine-epoxy addition, phase separation does not occur, likely due to the more homogeneous network formed during step-growth polymerization, counteracting phase separation between the crosslinking and non-crosslinking phases. These microgels demonstrated a more homogeneous internal structure with smaller meshed pores.[25]

In contrast to in-mold polymerization and photolithography, microfluidics can be operated continuously with the benefit of high production rates. While most microfluidic syntheses yield spherical microgels, more recent works have focused on preparing soft, rod-shaped microgels.[1,26,27] Rod-shaped microgels feature anisometry and, therefore, directionality, which is important for a variety of applications. Jammed microgel rods produce large open voids, due to their higher aspect ratio.[1] This macroscopic structure is beneficial for cell seeding, proliferation, cell-cell interactions, and the exchange of nutrients, rendering these jammed microgel rods interesting as injectable regenerative scaffolds. In addition, magneto-responsive rod-shaped microgels can be magnetically aligned inducing enhanced directionality and enabling oriented cell growth, a requirement for scaffolds aiming at the growth of nerves or muscle tissue.[28] While the magnetic alignment of the microgel rods is well understood, the effect of their internal structure and mechanical properties on their organization on the colloidal level when assembled and interlinked to form a tissue-engineering scaffold is not yet clarified.

Rod-shaped microgels, produced via droplet microfluidics, exhibit Young's moduli between 1.8 to 10 kPa (measured via nanoindentation using atomic force microscopy (AFM)) for PEG concentrations ranging from 2 % to 3 % (w/v) when crosslinked via Michael-type addition.[29] This is around 10 to 18-fold higher, compared to the storage modulus of bulk hydrogels prepared with the same polymer composition and reaction mechanism, as determined by rheology. In the case of free-radical photo-polymerization of rod-shaped microgels, the UV dose (intensity and time) on chip will also affect the internal structure.[1] Moreover, the addition of charged co-monomers significantly increases the swellability and reduces the stiffness of rod-shaped PEG microgels.[1]

In this report, we aim to gain understanding of the different parameters that affect the internal structure of rod-shaped micron-scaled microgels produced via microfluidics versus bulk hydrogels, both crosslinked via free-radical polymerization. We perform systematic characterization by varying the concentration, molar mass, and ratio of 8-arm star-shaped PEG-acrylate (sPEG-Ac) and PEG-DA components.[30] Different ratios of 8-arm sPEG-Ac with molar masses of 10 kDa and 20 kDa in combination with a lower molar mass PEG-DA (700 Da) are tested to produce microgels and bulk hydrogels, which we analyse in terms of their diffusivity, morphology, chemical functionality, and mechanical properties. Bulk hydrogels are produced as reference materials, crosslinked using comparable conditions as in microfluidics. We also investigate the interaction of the rod-shaped microgels with cells by modifying the microgels with H-Gly-Arg-Gly-Asp-Ser-Pro-Cys-OH (GRGDS-PC) as a cell adhesive peptide, and we correlate these results with the physical and mechanical properties of the microgels' network. The gained knowledge will allow us to better design and employ microgels as building blocks for applications, such as scaffold formation to grow cells in 3D and for engineered tissues.

Results and Discussion

Bulk hydrogels

We start by characterizing the gelation kinetics and the resulting mechanical properties of bulk hydrogels using rheology (see Figure 1a–b). The bulk hydrogels are produced by crosslinking pre-polymer solutions with a total amount of

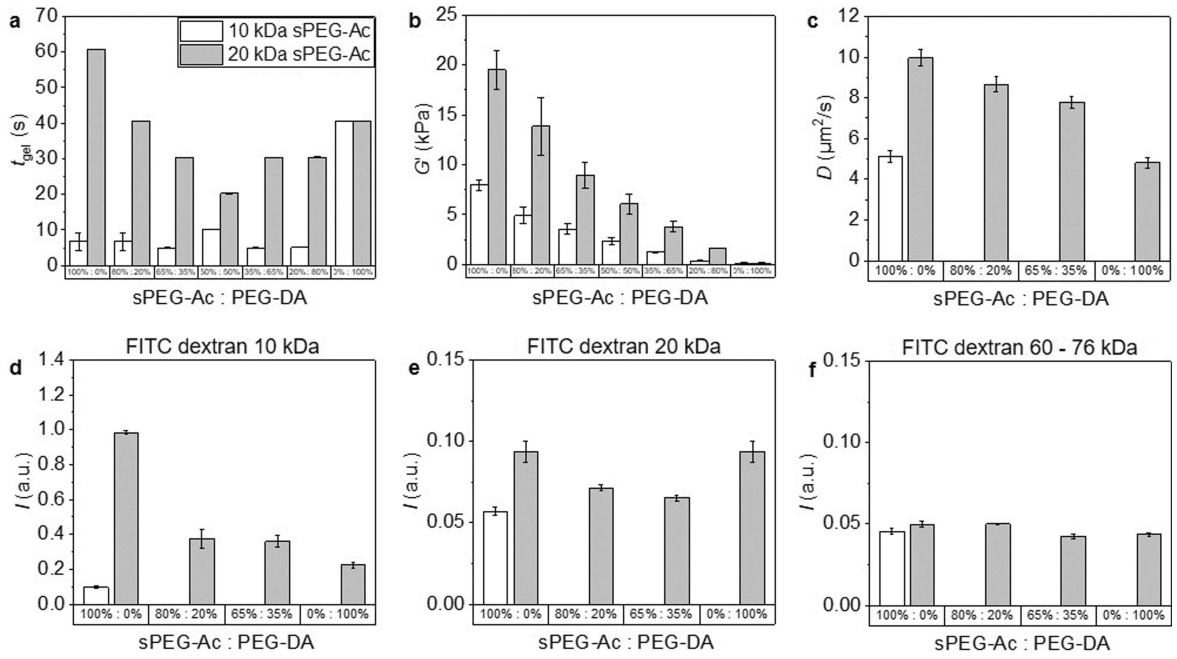

Figure 1. Characterization of pre-polymer solution and bulk hydrogels. Rheology measurements of samples with 5 wt% pre-polymer concentration and 50 mol% LAP containing mixtures of sPEG-Ac (10 kDa or 20 kDa) and PEG-DA: a) gelation time t_{gel}, and b) storage modulus G'. c) Diffusion coefficients D of FITC in bulk hydrogels are determined via FRAP method. Bulk hydrogels with a height of 100 μm are incubated with FITC-dextrans for 48 h. Normalized intensity I of FITC-dextrans d) 10 kDa, e) 20 kDa, and f) 60–76 kDa at a height of 0 μm (bottom of hydrogels) is measured in hydrogels with 5 wt% pre-polymer concentration and an irradiation dose of 467 mJ mm^{-2}. The intensity is normalized to the highest fluorescence intensity of FITC. Data is presented as mean ± s.d., n = 3 hydrogels.

5 wt% PEG, consisting of different ratios of 8-arm PEG-Ac (M_W = 10 kDa or 20 kDa) and PEG-DA (M_n = 700 Da), via free radical polymerization using 50 mol% of the photo-initiator lithium phenyl-2,4,6-trimethylbenzoylphosphinate (LAP) (with respect to the reactive acrylate groups) activated with a UV dose of 10 mW cm^{-2}. The absolute concentrations of the pre-polymer solutions used in the rheology measurements as well as for the synthesis of bulk hydrogels and microgels in the microfluidic set-up are shown in Table S1–S3, Supporting Information. The gelation time is determined by extrapolating to where the increasing storage modulus G' reaches the plateau. A suitable LAP concentration has been previously determined in microfluidic experiments as described in Section *materials and methods* and shown in Figure S1, Supporting Information.

As expected, decreasing the molar mass of 8-arm PEG-Ac from 20 to 10 kDa leads to faster gelation, simply because the number of reactive acrylate groups doubles when the overall PEG-Ac mass-concentration is kept constant (see Figure 1a). The successful gelation of a precursor solution only containing 8-arm PEG-Ac confirms that intermolecular links dominate the polymerization reaction.

While the combination of PEG-DA with 10 kDa sPEG-Ac does not significantly influence the gelation time t_{gel}, we observe shortening of t_{gel} when 20 kDa sPEG-Ac is mixed with PEG-DA up to a ratio of 50:50 by weight percent (see Figure 1a). Above 50% PEG-DA, t_{gel} increases again. Since 20 kDa sPEG-Ac has a larger coil volume of about 73×10^{-20} mL (as determined by intrinsic viscosity measurements, see Figure S2, Supporting Information), and therefore slower molecular diffusion compared to 10 kDa sPEG-Ac (coil volume = 8.5×10^{-20} mL), we believe that the shorter t_{gel} of the 20 kDa sPEG-Ac:PEG-DA system is the result of improved molecular diffusion by the short PEG-DA and the fact that in the presence of sPEG-Ac, fewer reactions are required to form a continuous gel network. With increasing ratio of PEG-DA above 50%, there are less sPEG-Ac crosslinker units in the solution, requiring more coupling steps before a continuous gel is achieved. By contrast, increasing amounts of PEG-DA do not affect the gelation rate of 10 kDa sPEG-Ac significantly, likely because 10 kDa sPEG-Ac has a smaller coil volume (8.5×10^{-20} mL, see Figure S2, Supporting Information) than the 20 kDa sPEG-Ac (73×10^{-20} mL) and its molecular diffusion is fast enough to rapidly form a stable polymer gel network. In the case of the pure PEG-DA system, very slow gelation kinetics occur compared to the mixed systems, due to the lack of multi-armed reactive precursors. It is important to note here that the effect of molecular diffusion, the number of reactive groups per molecule, and the total number of reactive acrylate groups in solution on the gelation process are difficult to decouple.

More surprisingly, we observe a higher G' in the 20 kDa sPEG-Ac systems compared to the 10 kDa sPEG-Ac (see Figure 1b). This is counterintuitive and could be explained by the density of the polymeric sPEG crosslinkers. While 20 kDa sPEG-Ac exhibits a bigger coil volume compared to

10 kDa sPEG-Ac, the 20 kDa sPEG-Ac has a significantly lower coil density of 45.6 mg mL^{-1} compared to the 10 kDa sPEG-Ac at 194.5 mg mL^{-1}, as determined by intrinsic viscosity measurements (see Figure S2, Supporting Information). Consequently, we believe that the 20 kDa sPEG-Ac may achieve greater conversion because of augmented accessibility of the reactive acrylate groups, leading to stiffer hydrogels. Single chain elasticity is inversely proportional to the chain length for an ideal polymer. Shorter chains can more easily interact with each other, which may contribute to a lowered mobility to crosslink with other molecules. For sPEG, the node in the centre of the molecules causes a high chain density, decreasing mobility in the core range. For the 20 kDa chains, however, the eight reactive groups are distributed on a higher effective surface due to the longer chains, while the chains themselves also have a higher flexibility, resulting in more crosslinks and thus a stiffer gel. The intra-polymer free volume increases with the polymer size for sPEG, resulting in easier diffusion of the small PEG-DA to fill up these pores and reducing diffusion of dextran through the network. Indeed, for both sPEG molecules, the addition of PEG-DA leads to a decrease of hydrogel stiffness down to few kPa (see Figure 1b). The softest hydrogels are obtained for 100 % PEG-DA after a long t_{gel} of 40 s, yielding a G' of only ≈0.14 kPa. The addition of PEG-DA to sPEG-Ac also influences the internal structure of the hydrogel, not only in terms of stiffness but also its diffusivity. Here, different hierarchical structures of the internal structure of hydrogels and microgels play a role when characterizing the stiffness and diffusion properties. Thereby, it is important to differentiate between i) macropores (≥50 μm)[31] that are formed during demixing upon polymerization,[32–34] ii) mesopores (2–50 nm)[31] that are formed due to crosslink density fluctuations and network inhomogeneities,[35,36] and iii) micropores (≤2 nm)[31] that reflect the free volume inside the polymer coils themselves,[37] and are highly dependent on the polymer and solvent.[38–40]

To investigate the internal structure, we produce bulk hydrogels as described above using a UV-LED (λ = 365 nm) with a dose of 467 mJ mm^{-2} and analyse the diffusion of differently sized fluorescein isothiocyanate (FITC)-dextrans through the bulk of the gels over a distance of 100 μm using confocal laser scanning microscopy (CLSM) (in height, z-direction in the coordinate system of the CLSM) (see Figure 1d-f). This allows us to probe the hydrogels for diffusion. Using FITC-dextrans with a size of 10 kDa, 20 kDa, or 60–76 kDa (stokes radii ≈2.3 nm, 3.3 nm, or 6.0 nm), we compare hydrogels produced from 100 % sPEG-Ac 20 kDa, mixtures of sPEG-Ac 20 kDa and PEG-Da (700 Da), or 100 % sPEG-Ac 10 kDa. As polymer mixtures made from sPEG-Ac 10 kDa and PEG-DA (700 Da) do not lead to stable microgels, we did not produce them as bulk hydrogels.

For the following data, the statistical analysis is shown in Figure S10, Supporting Information. The dextran diffusion is significantly reduced for 10 kDa; in fact, the diffusion in sPEG-Ac (10 kDa) is even slower than in pure PEG-DA hydrogels (see Figure 1d–f). Better diffusion properties are observed for 20 kDa sPEG-Ac, which indicates that more open space is available for 20 kDa than in 10 kDa sPEG-Ac hydrogels, likely due to the lower coil density. Furthermore, with increasing ratio of PEG-DA:sPEG-Ac (20 kDa) less diffusion takes place through the hydrogel, likely due to the fact that dangling, partially crosslinked PEG-DA molecules fill up the void space (in z-direction, see Figure 1d–f and Figure S3, Supporting Information).

Moreover, we determine the diffusion coefficient D of FITC in our hydrogels via fluorescence recovery after photobleaching (FRAP) (see Figure 1c). In agreement with the results of the just described macroscopic diffusion experiments, D determined by the FRAP experiments is lower for the hydrogels made from 10 kDa sPEG-Ac compared to the gels produced with 20 kDa sPEG-Ac. This confirms our previous hypothesis that the smaller molar mass sPEG-Ac exhibits more interchain interactions, while contributing less to crosslinking. Instead, smaller sPEG-Ac leads to more crowded meshes, and thus reduced diffusion. The higher coil density of the 10 kDa sPEG-Ac polymer seems to lead to steric hindrance and, therefore, blocked accessibility of reactive acrylate groups, resulting in only partially crosslinked polymer chains, hindering diffusion within the free volume (micropores) between the polymer chains. Also, we obtain lower D of FITC with increasing PEG-DA amount in the 20 kDa sPEG-Ac:PEG-DA system, while the lowest D is obtained for 100 % PEG-DA hydrogel (see Figure 1c). This suggests that an increased amount of PEG-DA leads to more crowded networks and less void space, due to the increased density of partially crosslinked PEG chains. Interestingly, 100 % sPEG-Ac (10 kDa) and pure PEG-DA hydrogels show comparable D (see Figure 1c). This demonstrates that the stiffer sPEG-Ac (10 kDa) and softer PEG-DA hydrogels exhibit similar steric hindrance, while the sPEG-Ac (10 kDa) results in more crosslinks. These results indicate that the addition of PEG-DA indeed leads to the presence of partially crosslinked polymer chains hindering the diffusion of molecules, while resulting in very soft hydrogels. Within this crowded network, the diffusion of the PEG chains will be reduced, so that for most molecules only one of the acrylate groups of PEG-DA becomes incorporated during polymerization. The dangling chain-ends fill up the pores of the hydrogel without increasing the crosslink density or stiffening of the network.

To verify this hypothesis (dangling polymer chains reduce the free volume and thus the diffusivity, while softening the gel due to less crosslinks and more free acrylates), we determine the amount of remaining reactive free acrylate groups inside the polymer network after photopolymerization. Bulk hydrogels are crosslinked with a UV dose of 467 mJ mm^{-2} for 30 sec, which mimics the exposure of the microgels. The free acrylates are quantified via Raman spectroscopy (see Figure S4, Supporting Information).

Thereby, the hydrogels are freeze-dried and the solid powder is measured, which allows for the detection of the acrylate groups throughout the whole polymer network. The individual peaks representing the acrylate groups, as well as C–C bonds of the PEG units enables the qualitative as well

as quantitative analysis of the acrylate groups related to C–C PEG units presented in the hydrogel polymer network. As already indicated, we measure a significantly higher ratio of free acrylate groups with respect to C–C PEG units for hydrogels made from sPEG-Ac (10 kDa) (24.2 %) compared to sPEG-Ac (20 kDa) (2.3 %) (see Table S4, Supporting Information) based on the calibration of free acrylate groups (see Figure S4a–c, Supporting Information). More free acrylate groups are also present with increasing PEG-DA amount, entailing the reduced diffusivity. The addition of PEG-DA to sPEG-Ac (20 kDa) increases the amount of free acrylate groups from 2.3 % to 35.4 % and 35.5 % (for 20 % and 35 % PEG-DA, respectively), which is consistent with the decreasing stiffness of the polymer networks (see Table S4, Supporting Information). This results are in line with a previous report where reducing the fraction of PEG-DA and increasing the amount of star-shaped polymer stabilizes the hydrogel network by connecting multiple polymer backbones together, increasing the stiffness.[41]

Rod-shaped microgels produced via microfluidics

After analysis of the internal structures of the bulk hydrogel systems, we now produce rod-shaped microgels with the same precursor solutions. The microgels are made by continuous on-chip gelation of droplets produced in the plug-flow regime of a microfluidic channel device (Scheme 1). The precursor solution is broken up into elongated droplets with a length of approximately 300 µm and subsequently UV crosslinked inside of the microfluidic channels, affording anisometric, rod-shaped microgels that are collected off-chip, as described previously.[1] Sufficient crosslinking on chip is essential to maintain the shape of the rod-shaped microgels after they exit the chip. To induce rapid gelation, the water-soluble LAP radical-photo-initiator is mixed with the precursor molecules (sPEG-Ac, PEG-DA). Depending on the molar mass and concentration of sPEG-Ac, the required t_{gel}—during which polymerization and crosslinking occurs to form the microgel rods—varies. To ensure that the microgels are fully crosslinked for all tested precursor solutions, we irradiate continuously at a maximum power of 300 mW leading to a dose of 467 mJ mm^{-2} for each droplet or microgel, as we maintain the flow rates for the dispersed and continuous phases identical at $V'_{disp} = 35\ \mu L\,h^{-1}$ and $V'_{cont} = 35\ \mu L\,h^{-1}$. This leads to a rate of around 220 droplets per minute.

Using this set-up, we produce microgels with 100 % sPEG-Ac (10 kDa), 100 % sPEG-Ac (20 kDa), 80 % sPEG-Ac (20 kDa)—20 % PEG-DA, and 65 % sPEG-Ac (20 kDa)—35 % PEG-DA, while maintaining a constant total precursor concentration of 5 wt %. At this concentration, a combination of PEG-DA and sPEG-Ac (10 kDa) does not lead to stable microgels under the tested conditions. For the following data, the statistical analysis is shown in Figure S11, Supporting Information. Microgels with higher molar mass sPEG-Ac (20 kDa) show significantly higher stiffness (higher effective Young's modulus E_{eff}) compared to lower molar mass sPEG-Ac (10 kDa) in nanoindentation measurements (see Figure 2a). In addition, D of FITC is significantly higher in microgels made from 20 kDa sPEG-Ac compared to the 10 kDa homologue (see Figure 2b). These trends correlate with the observations made in bulk hydrogels. Moreover, the E_{eff} of the microgels

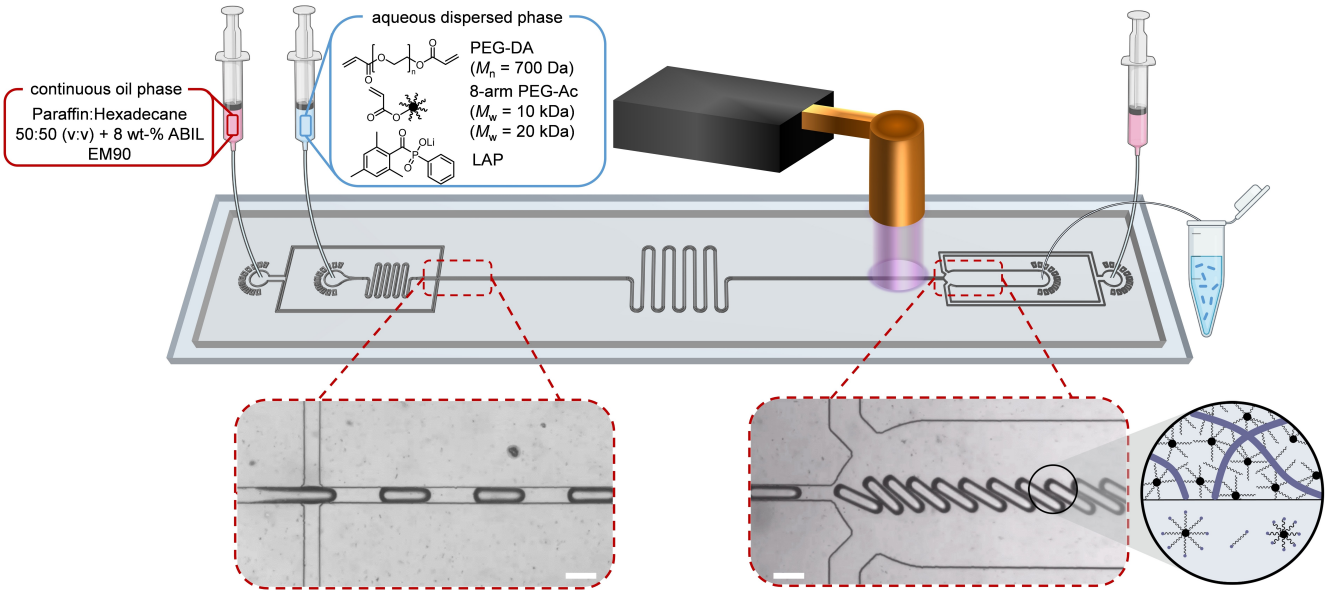

Scheme 1. Schematic microfluidic chip design for continuous plug-flow on-chip production of rod-shaped microgels. Red syringes show the inlets for first (for pinching-off the dispersed droplets) and second continuous phase (before outlet for diluting or separating of the polymerized microgel rods). Blue syringe indicates the inlets for the dispersed phase. The purple shading represents the UV irradiation on chip. Dashed inserts represent brightfield images of characteristic section of the microfluidic chip taken during operation. Scale bars represent 100 µm. (Created with BioRender.com)

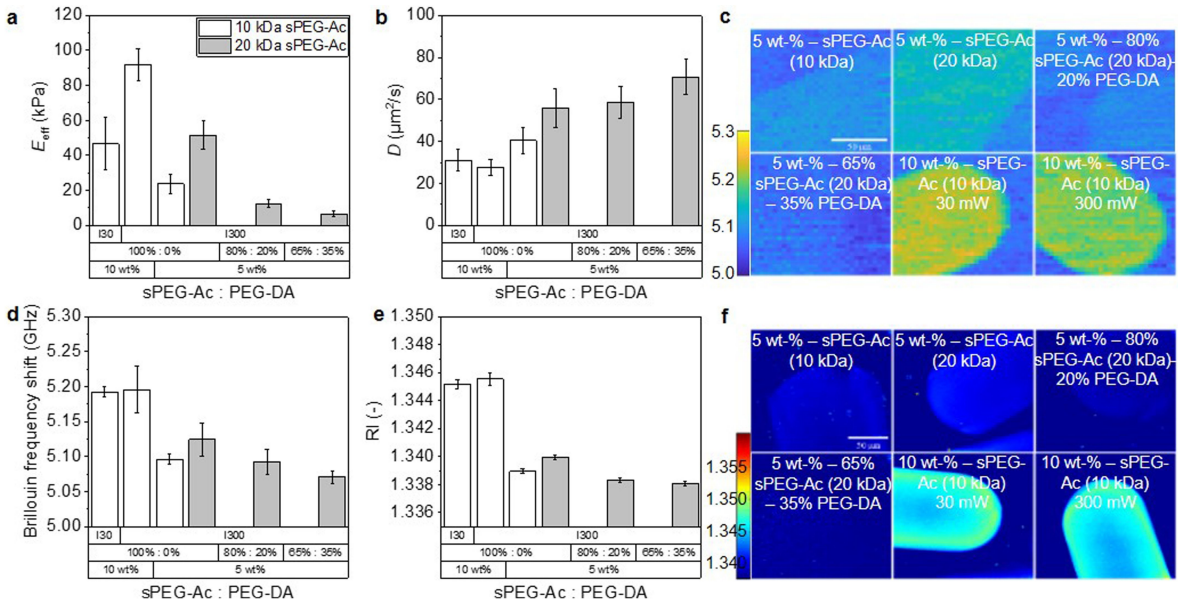

Figure 2. Characterization of rod-shaped microgels produced in plug-flow on-chip microfluidics. a) Effective Young's moduli E_{eff} of microgels is determined via nanoindentation measurements. Data is presented as mean ± s.d., n = 15 microgels per type at a minimum of 3 different locations. b) Diffusion coefficient D of FITC in the microgels is determined via FRAP method. c) Brillouin frequency shift maps, d) Brillouin frequency shift measurements, e) Refractive indices (RI) and f) tomographic RI reconstructions of microgels with different polymer compositions. Data is presented as mean ± s.d., n = 5 microgels. Scale bars represent 50 µm.

decreases with increasing amounts of PEG-DA in the sPEG-Ac (20 kDa) system. Interestingly, in contrast to the bulk hydrogels, diffusion of FITC slightly increases with the addition of PEG-DA to sPEG-Ac (20 kDa). This suggests that the internal structure of the microgels is different from the bulk hydrogels. The difference may arise from polymerization in the confined spaces of the droplets in microfluidics and different polymer thickness of the bulk hydrogels.

To better understand the correlation between the mechanical and diffusion properties, we perform Brillouin microscopy and optical diffraction tomography (ODT) measurements (see Figure 2c–f). Brillouin microscopy is a powerful technique to provide label-free, non-contact, and spatially resolved measurements of the mechanical properties of biological samples,[42–44] but it has also been employed for microgels.[45–48] The Brillouin frequency shift is measured, which is related to the longitudinal modulus, refractive index (RI), and the absolute density of the sample.[44] The longitudinal modulus determines the compressibility of the samples. The ODT measures RI of the samples, which is linearly proportional to the mass density of most biological samples and microgels.[46,49] We observe a higher Brillouin frequency shift and RI for the 20 kDa compared to the 10 kDa microgels. Here, higher RI of the 20 kDa sample indicates that the microgels contain less water, due to less swelling, which is in agreement with the higher crosslinking density based on the higher stiffness of the sPEG-Ac (20 kDa) microgels, measured by nanoindentation.[44] The addition of PEG-DA added to sPEG-Ac (20 kDa) leads to a decrease of Brillouin frequency shift and RI, while no significant difference can be observed between 20 % or 35 % of added PEG-DA. This decrease in the Brillouin frequency shift and RI indicates a lower crosslink density, which is corroborated by the slightly improved diffusion when PEG-DA is added.

Furthermore, we investigate our microgels using cryo-SEM (scanning electron microscopy). We observe more crude structures for the 20 kDa microgels, while the structure of 10 kDa appears more defined (see Figure S5, Supporting Information). This is in agreement with the diffusion studies that indicate overall larger mesh sizes for the 20 kDa microgels, while for the 10 kDa partially crosslinked polymer chains may hinder molecule diffusion. To corroborate that indeed larger hierarchical pores are formed for the 20 kDa sample, we characterize the macroporosity of the 20 kDa and 10 kDa sPEG-Ac microgels using STED (Stimulated Emission Depletion) microscopy followed by image analysis (see Figure S6, Supporting Information). In the obtained porosity histogram, we observe larger macroscopic pores with radii up to 200 nm and 76.5 % of the pores having a radius below 120 nm for the 20 kDa compared to the 10 kDa microgels, where 92.8 % of the pores have a radius lower than 120 nm. This explains the results from the local D measurements by FRAP in microgels in Figure 2b, but also the macroscopic diffusion experiments with fluorescent dextrans in the bulk hydrogels (see Figure 1d–f). The clear phase separation for the 20 kDa polymer network can occur due to lower solubility of the higher molar mass 20 kDa in solvent compared to the 10 kDa homologue.

To better investigate the effect of a lower UV dose on the mechanical and diffusion properties of the microgels, we crosslink the same droplets of polymer precursor with 10 wt % sPEG-Ac (10 kDa) using a UV-LED of 300 mW (dose = 467 mJ mm^{-2}) or 30 mW (dose = 46.7 mJ mm^{-2}). This

concentration is chosen because it allows production of stiffer crosslinked, stable microgels that are irradiated with a very low UV light power of 30 mW. Microgels, irradiated with this lower power (30 mW) show a significantly lower E_{eff}. However, the diffusion properties of both microgels are not significantly different. Again, to better understand the correlation between the mechanical and diffusion properties, we perform Brillouin microscopy and RI measurements (see Figure 2c–f). We observe similar Brillouin frequency shifts (see Figure 2d) for microgels irradiated with 30 mW or 300 mW, but higher RI for the microgels irradiated at 300 mW (see Figure 2e). Interestingly, the microgels irradiated at the higher power of 300 mW exhibit higher RI at the periphery of the microgels. Furthermore, both conditions exhibit a similar amount of reactive acrylate groups measured via Raman spectroscopy (see Table S4 and Figure S4, Supporting Information). The RI and E_{eff} of microgels irradiated with higher power suggest that the crosslinking density is higher at the periphery as the E_{eff} is measured at the surface of the microgels. However, the similar Brillouin frequency shift, diffusion properties, and amount of reactive acrylate groups indicate that the overall polymer network structure is similar for both conditions. Moreover, 10 wt % microgels made from sPEG-Ac (10 kDa) show a higher Brillouin frequency shift and RI compared to 5 wt % microgels, which is consistent with the increase in stiffness and reduced diffusion. In general, the 5 wt % samples show homogeneous structures in the Brillouin frequency shift maps (see Figure 2c) and tomographic RI reconstruction images (see Figure 2f). Interestingly, the 10 wt % microgels show slightly higher RI at the periphery of the rod-shaped microgels compared to the core (see Figure 2f), which can be explained by stronger crosslinking at the interfaces, typical for photopolymerization reactions.

Cell culture

We have shown how the variation of molecular building blocks influence the internal structure of rod-shaped microgels, which affects the mechanical and diffusion properties of the material, both playing a major role in 3D cell culture. In this report, the biocompatibility and cell-adhesiveness of selected microgels is shown in 2.5D cell culture experiments using L929 mouse fibroblasts.

To introduce cell adhesion peptides to the microgels and render them suitable for cell culture, we post-functionalize our rod-shaped microgels with GRGDS-PC using thiol-Michael addition of cysteine (present in the peptide) with the free acrylate groups of the microgel.

To characterize cell-microgel interactions, the microgels are seeded with L929 mouse fibroblasts. Cell attachment depends on the microgel stiffness and the accessibility of RGD binding domain in GRGDS-PC, and is characterized via live imaging of at least 7 microgels per condition during 120 min after cell seeding at 37 °C, 5 % CO_2 in humid environment (see Figure 3 and Figure S7, Supporting Information). We observe several filopodial protrusion of cells on 5 wt % sPEG-Ac (20 kDa) microgels, which indicates initiated cell adhesion. Moreover, fully spread cells can be observed on 10 wt % sPEG-Ac (10 kDa) microgels (dose = 46.7 mJ mm^{-2}, 30 mW UV-LED power irradiation). Both these microgels have a similar elastic modulus around 50 kPa thus the difference in cell spreading is likely due to variable accessibility of RGD (see Figure 2a). On elastic hydrogels, cell spreading is usually enhanced on stiffer gels.[50] However, in the case of stiffer 10 wt % sPEG-Ac (10 kDa) (dose = 467 mJ mm^{-2}, $E_{eff} \approx 92$ kPa), we observe no stable cell attachment.

To better understand cell attachment on the different microgels, we characterize the amount of GRGDS-PC incorporated into the polymeric network of the microgels via XPS (X-Ray Photoelectron Spectroscopy) analysis (see Table S5, Supporting Information). We measure the nitrogen-to-carbon (N/C) ratio as only the peptide contains nitrogen and thus this ratio indicates how much peptide is coupled to the microgels. The highest N/C ratio of 8.1 % is observed for the microgels with best cell attachment (10 wt % sPEG-Ac (10 kDa) (46.7 mJ mm^{-2}). Moreover, microgels with 5 wt % sPEG-Ac (20 kDa) exhibit 2.1 % N/C ratio, which may explain the observed low number of attached but rounded cells. All other microgel types do not show considerable cell attachment after 120 min, in agreement with the XPS results where no GRGDS-PC peptides could be detected on these microgels. Microgels with higher PEG-DA amount (5 wt % — 65 % sPEG-Ac (20 kDa) — 35 % PEG-DA) dissolve in ethanol when sterilized and can therefore not be used for cell culture experiments. It is surprising that cell attachment failed for microgels irradiated with higher power (10 wt % sPEG-Ac (10 kDa) (467 mJ mm^{-2})) as an N/C ratio of 6.3 % is observed (see Table S5, Supporting Information). This is lower compared to 10 wt % sPEG-Ac (10 kDa, 46.7 mJ mm^{-2}) microgels but higher than 5 wt % sPEG-Ac (20 kDa) microgels (dose = 467 mJ mm^{-2}). A reason for this observation could be the presence of the RGD on the outside of the microgels. In microfluidic technique, we assume more crosslinking at the outside of the microgels and thus less free acrylates to couple the peptide. This effect is probably stronger for the higher dose in the 10 wt % system, and in the case of a higher crosslinking density for 20 kDa sPEG in comparison to the 10 kDa sPEG-Ac due to less steric hindrance of the polymer. The significantly lower percentage of free acrylate groups for the sPEG-Ac (20 kDa) microgels also explains the lower concentration of coupled peptide.

In a next step, we seed L929 fibroblasts on the microgels and culture them for 1 or 2 days (see Figure 4), after which the cells are fixed and their nucleus and actin filaments are fluorescently labelled with DAPI and Phalloidin594, respectively, to image cell spreading. This experiment is performed in triplicate and we analyse more than 30 microgels per condition. As indicated by the live imaging, cell protrusion on the 5 wt % sPEG-Ac (20 kDa) microgels started after 120 min, but after 2 days of culture, the cells still look round and clustered. For the 5 wt % sPEG-Ac (10 kDa) microgels, there is attachment of several round cells after 1 day of culture — with some cells starting to spread, while on day 2, the cells are mostly spread on the microgel surface. For the

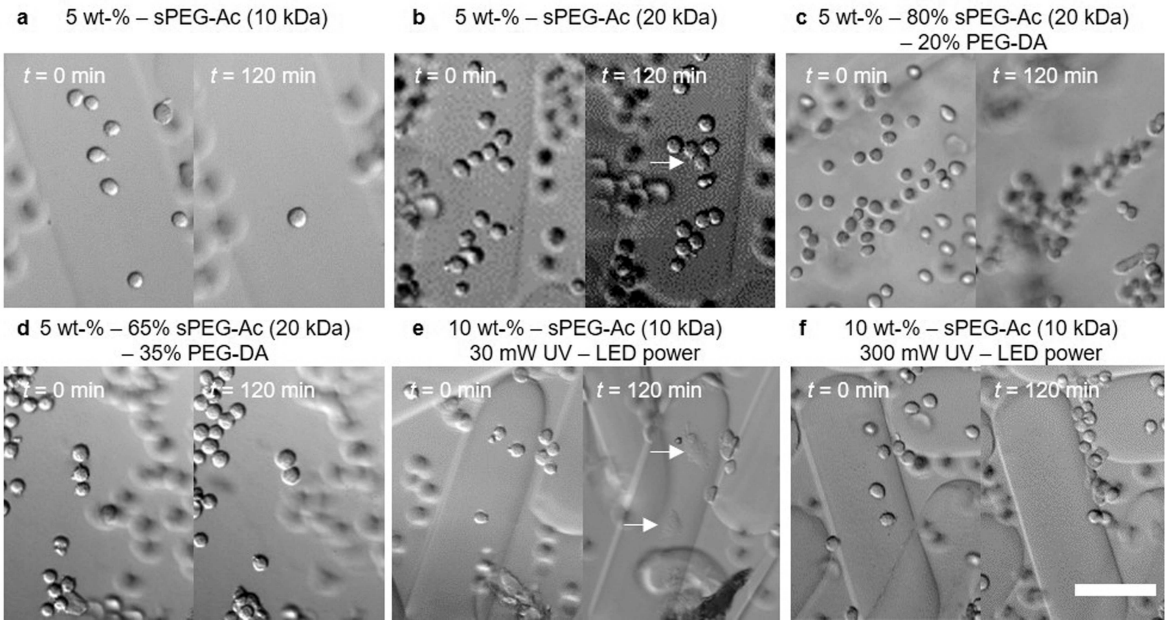

Figure 3. L929 fibroblast adhesion on most representative single rod-shaped microgels. Microgels ($n > 7$) are post-functionalized with GRGDS-PC. Images of live imaging of the microgels a) 5 wt%—100% sPEG-Ac (10 kDa)—0% PEG-DA, b) 5 wt%—100% sPEG-Ac (20 kDa)—0% PEG-DA, c) 5 wt%—80% sPEG-Ac (20 kDa)—20% PEG-DA, d) 5 wt%—65% sPEG-Ac (20 kDa)—35% PEG-DA, e) 10 wt%—sPEG-Ac (10 kDa)—0% PEG-DA, 30 mW UV-LED power, and f) 10 wt%—sPEG-Ac (10 kDa)—0% PEG-DA, 300 mW UV-LED power are taken via differential interference contract (DIC) microscopy at $t = 0$ min and $t = 120$ min. White arrowheads show filopodial protrusion, which indicates cell-microgel interaction. 5 wt%—sPEG-Ac (20 kDa) microgels show several filopodial protrusion, while for 10 wt%—sPEG-Ac (10 kDa) (30 mW UV-LED power) microgels a larger number of filopodial protrusion can be observed. Cell attachment for the other microgel samples show more rounded cells after $t = 120$ min. Scale bar represents 100 μm.

5 wt%—80% sPEG-Ac (20 kDa)—20% PEG-DA microgels, there is only attachment of several round cells after 1 day of culture, while after 2 days cluster formation on the microgels can be observed. This is a typical observation when cells do not interact well with the substrate. Then they produce extracellular matrix proteins as a rescue mechanism and interact with each other instead of the substrate. Interestingly, the 10 wt% sPEG-Ac (10 kDa) (30 mW UV-LED power irradiation) microgels strongly support cell proliferation on the microgels surface already after 1 day, while after 2 days of culture, the cells spread over the entire microgel surface (see Figure 4).

The microgels exposed to 300 mW UV-LED do not support any cell attachment, even after 2 days, likely due to the highly crosslinked surface, not allowing the peptide GRGDS-PC to bind there. To better understand the mechanobiology on the 10 wt% sPEG-Ac (10 kDa) (30 mW UV-LED power irradiation) microgels, we immunostain the Yes-associated protein (YAP) as it shows an intracellular localization, which can be correlated to how well cells interact with their substrate. YAP is predominantly in the cell nucleus when cells are grown and spreading nicely on stiff substrates (50 kPa).[51–53] Supporting previously published trends, we observe predominant localization of YAP in the cell nucleus for our 10 wt% sPEG-Ac (10 kDa) (30 mW UV-LED power irradiation) microgels (see Figure S8, Supporting Information).[51,52]

Besides stiffness, it has already been reported that the viscoelasticity of hydrogels can significantly influence cell-material interaction.[54–56] Recent work has revealed that viscoelasticity of a material can regulate fundamental cell behaviour, such as spreading, growth, proliferation, migration, and differentiation, enabling cells to spread also on softer viscoelastic hydrogels.[56] Therefore, we characterize the storage modulus G' and loss modulus G'' of the microgels as shown in Figure S9, Supporting Information. The viscoelastic behaviour of the microgels is evaluated by the parameter tan δ that describes the ratio between G'' to G', while for tan $\delta < 1$, the elastic and for tan $\delta > 1$, the viscous part of the material is dominant. We observe similar tan δ for all microgels in a range of tan $\delta = 0.1$–0.2, which means that the microgels are elastic and that mainly the accessibility of the RGD peptide influences cell adhesion, spreading, and proliferation.

Conclusion

In this study, we obtain better understanding of how the internal structure of soft rod-shaped microgels in comparison to bulk hydrogels can be affected by changing different parameters of the molecular building blocks. This internal structure influences both the stiffness and the diffusion properties of molecules throughout the gels. We also demonstrate that the microgels can support cell spreading

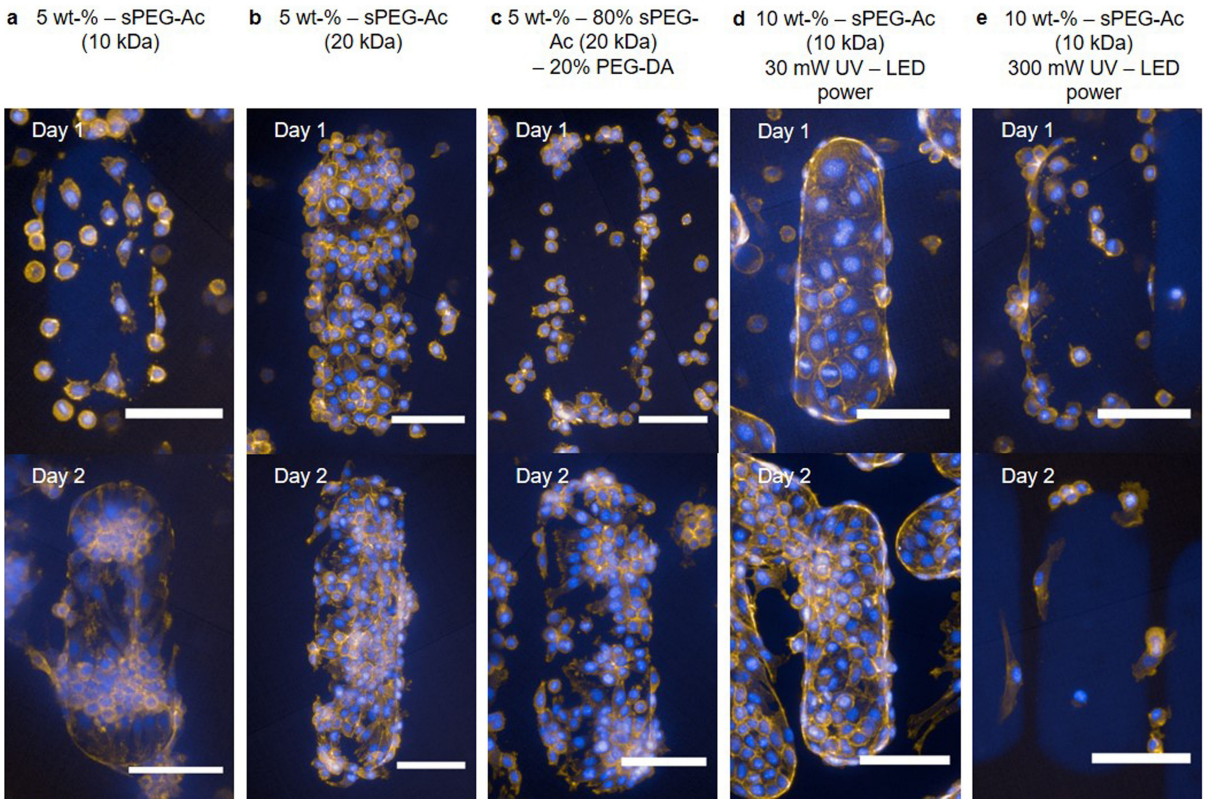

Figure 4. L929 cell-microgel interaction. Fluorescent confocal images show cell attachment and spreading on microgels ($n > 30$) a) 5 wt%—100% sPEG-Ac (10 kDa)—0% PEG-DA, b) 5 wt%—100% sPEG-Ac (20 kDa)—0% PEG-DA, c) 5 wt%—80% sPEG-Ac (20 kDa)—20% PEG-DA, d) 10 wt%—sPEG-Ac (10 kDa)—0% PEG-DA, 30 mW UV-LED power, and e) 10 wt%—sPEG-Ac (10 kDa)—0% PEG-DA, 300 mW UV-LED power after 1 day and 2 days of culture. Cell nuclei and actin filament are fluorescently labelled with DAPI (blue) and Phalloidin594 (yellow), respectively. Scale bars represent 100 µm.

and growth and that this mainly depends on how efficiently the cell adhesive peptide GRGDS-PC can be coupled to the free acrylates on the microgel surface.

In conclusion, our findings represent a roadmap to design rod-shaped microgels for tissue engineering or drug delivery applications, to vary their internal structures and obtain the desired stiffness and diffusion properties for nutrients and other bioactive molecules. Furthermore, our microgels can easily be modified with biological or chemical functional groups. They can be used for the synthesis of 3D macroporous constructs that allow for 3D cell culture and tissue growth.

Acknowledgements

This work was funded by the collaborative research center (CRC) on microgels SFB 985 project B5 and C3 from DFG (Deutsche Forschungsgemeinschaft). Furthermore, the authors acknowledge financial support from the European Research Council within the ERC-2021-COG project 101043656, Heartbeat. We thank Laura Klasen for her help with the ToC image. Moreover, we thank Joachim Roes for the XPS measurements and Dr. Özge Ekin Akdere for her help with the cell culture experiments. Open Access funding enabled and organized by Projekt DEAL.

Conflict of Interest

The authors declare no conflict of interest.

Data Availability Statement

The data that support the findings of this study are available from the corresponding author upon reasonable request.

Keywords: Diffusion · Internal Structure · Mechanical Properties · Microfluidics · PEG Microgels

[1] D. Rommel, M. Mork, S. Vedaraman, C. Bastard, L. P. B. Guerzoni, Y. Kittel, R. Vinokur, N. Born, T. Haraszti, L. De Laporte, *Adv. Sci.* **2022**, *9*, 2103554.
[2] V. K. Switacz, S. K. Wypysek, R. Degen, J. J. Crassous, M. Spehr, W. Richtering, *Biomacromolecules* **2020**, *21*, 4532–4544.
[3] M. Zhong, R. Wang, K. Kawamoto, B. D. Olsen, J. A. Johnson, *Science* **2016**, *353*, 1264–1268.
[4] L. De Keer, K. I. Kilic, P. H. M. Van Steenberge, L. Daelemans, D. Kodura, H. Frisch, K. De Clerck, M. F. Reyniers, C. Barner-Kowollik, R. H. Dauskardt, D. R. D'hooge, *Nat. Mater.* **2021**, *20*, 1422–1430.
[5] O. Yom-Tov, D. Seliktar, H. Bianco-Peled, *Eur. Polym. J.* **2016**, *74*, 1–12.

[6] C. R. Nuttelman, M. A. Rice, A. E. Rydholm, C. N. Salinas, D. N. Shah, K. S. Anseth, *Prog. Polym. Sci.* **2008**, *33*, 167–179.
[7] Y. Kittel, A. J. C. Kuehne, L. De Laporte, *Adv. Healthcare Mater.* **2021**, *10*, 2101989.
[8] R. A. Meurer, S. Kemper, S. Knopp, T. Eichert, F. Jakob, H. E. Goldbach, U. Schwaneberg, A. Pich, *Angew. Chem. Int. Ed.* **2017**, *56*, 7380–7386.
[9] E. Axpe, D. Chan, G. S. Offeddu, Y. Chang, D. Merida, H. L. Hernandez, E. A. Appel, *Macromolecules* **2019**, *52*, 6889–6897.
[10] Y. Tsuji, X. Li, M. Shibayama, *Gels* **2018**, *4*, 50.
[11] V. Hagel, T. Haraszti, H. Boehm, *Biointerphases* **2013**, *8*, 36.
[12] T. Yang, M. Malkoch, A. Hult, *J. Polym. Sci. Part A* **2013**, *51*, 1378–1386.
[13] S. P. Zustiak, H. Boukari, J. B. Leach, *Soft Matter* **2010**, *6*, 3609–3618.
[14] M. S. Rehmann, K. M. Skeens, P. M. Kharkar, E. M. Ford, E. Maverakis, K. H. Lee, A. M. Kloxin, *Biomacromolecules* **2017**, *18*, 3131–3142.
[15] M. E. Hwang, P. J. Black, C. D. Elliston, B. A. Wolthuis, D. R. Smith, C. C. Wu, S. Wenske, I. Deutsch, *Radiat. Oncol.* **2018**, *13*, 192.
[16] A. D. Rao, Z. Feng, E. J. Shin, J. He, K. M. Waters, S. Coquia, R. DeJong, L. M. Rosati, L. Su, D. Li, J. Jackson, S. Clark, J. Schultz, D. Hutchings, S.-H. Kim, R. H. Hruban, T. L. DeWeese, J. Wong, A. Narang, J. M. Herman, K. Ding, *Int. J. Radiat. Oncol. Biol. Phys.* **2017**, *99*, 1111–1120.
[17] S. Vaggers, B. P. Rai, E. C. P. Chedgy, A. de la Taille, B. K. Somani, *World J. Urol.* **2021**, *39*, 1769–1780.
[18] S. Lee, X. Tong, F. Yang, *Biomater. Sci.* **2016**, *4*, 405–411.
[19] T. Rossow, J. A. Heyman, A. J. Ehrlicher, A. Langhoff, D. A. Weitz, R. Haag, S. Seiffert, *J. Am. Chem. Soc.* **2012**, *134*, 4983–4989.
[20] K. H. Son, J. W. Lee, *Materials* **2016**, *9*, 854.
[21] A. J. D. Krüger, J. Köhler, S. Cichosz, J. C. Rose, D. B. Gehlen, T. Haraszti, M. Möller, L. De Laporte, *Chem. Commun.* **2018**, *54*, 6943–6946.
[22] A. J. D. Krüger, O. Bakirman, L. P. B. Guerzoni, A. Jans, D. B. Gehlen, D. Rommel, T. Haraszti, A. J. C. Kuehne, L. De Laporte, *Adv. Mater.* **2019**, *31*, 1903668.
[23] H. J. M. Wolff, J. Linkhorst, T. Göttlich, J. Savinsky, A. J. D. Krüger, L. De Laporte, M. Wessling, *Lab Chip* **2020**, *20*, 285–295.
[24] S. Boesveld, A. Jans, D. Rommel, M. Bartneck, M. Möller, L. Elling, C. Trautwein, P. Strnad, A. J. C. Kuehne, *ACS Appl. Mater. Interfaces* **2019**, *11*, 25017–25023.
[25] J. C. Rose, M. Cámara-Torres, K. Rahimi, J. Köhler, M. Möller, L. De Laporte, *Nano Lett.* **2017**, *17*, 3782–3791.
[26] A. C. Suturin, A. J. D. Krüger, K. Neidig, N. Klos, N. Dolfen, M. Bund, T. Gronemann, R. Sebers, A. Manukanc, G. Yazdani, et al., *Adv. Healthcare Mater.* **2022**, *11*, 2200989.
[27] D. L. Braunmiller, S. Babu, D. B. Gehlen, M. Seuß, T. Haraszti, A. Falkenstein, J. Eigen, L. De Laporte, J. J. Crassous, *Adv. Funct. Mater.* **2022**, *32*, 2202430.
[28] J. C. Rose, M. Fölster, L. Kivilip, J. L. Gerardo-Nava, E. E. Jaekel, D. B. Gehlen, W. Rohlfs, L. De Laporte, *Polym. Chem.* **2020**, *11*, 496–507.
[29] L. P. B. Guerzoni, J. C. Rose, D. B. Gehlen, A. Jans, T. Haraszti, M. Wessling, A. J. C. Kuehne, L. De Laporte, *Small* **2019**, *15*, 1900692.
[30] Z. Zhang, A. Loebus, G. De Vicente, F. Ren, M. Arafeh, Z. Ouyang, M. C. Lensen, *Polymer* **2018**, *10*, 970.
[31] Y. Fukumori, H. Takeuchi, Y. Ando in *Nanoparticle Technology Handbook* (Eds.: M. Naito, T. Yokoyama, K. Hosokawa, K. Nogi), Elsevier, Amsterdam, **2018**, pp. 49–107.
[32] C. Fernández-Rico, T. Sai, A. Sicher, R. W. Style, E. R. Dufresne, *JACS Au* **2022**, *2*, 66–73.
[33] F. Wang, L. Ratke, H. Zhang, P. Altschuh, B. Nestler, *J. Sol-Gel Sci. Technol.* **2020**, *94*, 356–374.
[34] R. W. Style, T. Sai, N. Fanelli, M. Ijavi, K. Smith-Mannschott, Q. Xu, L. A. Wilen, E. R. Dufresne, *Phys. Rev. X* **2018**, *8*, 011028.
[35] Z. Tang, L. Jiang, *Giant* **2022**, *12*, 100131.
[36] S. Seiffert, *Polym. Chem.* **2017**, *8*, 4472–4487.
[37] V. P. Swapna, V. S. Abhisha, R. Stephen in *Polymer Nanocomposite Membranes for Pervaporation* (Eds.: S. Thomas, S. C. George, T. Jose), Elsevier, Amsterdam, **2020**, pp. 201–229.
[38] S. M. Fica-Contreras, D. J. Hoffman, J. Pan, C. Liang, M. D. Fayer, *J. Am. Chem. Soc.* **2021**, *143*, 3583–3594.
[39] J. Pacułt, M. Rams-Baron, B. Chrząszcz, R. Jachowicz, M. Paluch, *Mol. Pharmaceutics* **2018**, *15*, 2807–2815.
[40] X. Han, J. Gao, T. Chen, L. Qian, H. Xiong, Z. Chen, *Nanomaterials* **2022**, *12*, 4161.
[41] C. C. Lin, K. S. Anseth, *Pharm. Res.* **2009**, *26*, 631–643.
[42] G. Scarcelli, W. J. Polacheck, H. T. Nia, K. Patel, A. J. Grodzinsky, R. D. Kamm, S. H. Yun, *Nat. Methods* **2015**, *12*, 1132–1134.
[43] R. Prevedel, A. Diz-Muñoz, G. Ruocco, G. Antonacci, *Nat. Methods* **2019**, *16*, 969–977.
[44] R. Schlüßler, K. Kim, M. Nötzel, A. Taubenberger, S. Abuhattum, T. Beck, P. Müller, S. Maharana, G. Cojoc, S. Girardo, et al., *eLife* **2022**, *11*, e68490.
[45] A. J. Traverso, J. V. Thompson, Z. A. Steelman, Z. Meng, M. O. Scully, V. V. Yakovlev, *Anal. Chem.* **2015**, *87*, 7519–7523.
[46] S. Girardo, N. Träber, K. Wagner, G. Cojoc, C. Herold, R. Goswami, R. Schlüßler, S. Abuhattum, A. Taubenberger, F. Reichel, D. Mokbel, M. Herbig, M. Schürmann, P. Müller, T. Heida, A. Jacobi, E. Ulbricht, J. Thiele, C. Werner, J. Guck, *J. Mater. Chem. B* **2018**, *6*, 6245–6261.
[47] M. Bailey, M. Alunni-Cardinali, N. Correa, S. Caponi, T. Holsgrove, H. Barr, N. Stone, C. P. Winlove, D. Fioretto, F. Palombo, *Sci. Adv.* **2020**, *6*, eabc1937.
[48] N. Hauck, T. Beck, G. Cojoc, R. Schlüßler, S. Ahmed, I. Raguzin, M. Mayer, J. Schubert, P. Müller, J. Guck, et al., *Mater Adv* **2022**, *3*, 6179–6190.
[49] R. Barer, *Nature* **1952**, *169*, 366–367.
[50] R. Sunyer, A. J. Jin, R. Nossal, D. L. Sackett, *PLoS One* **2012**, *7*, e46107.
[51] Y. Chandorkar, A. Castro Nava, S. Schweizerhof, M. Van Dongen, T. Haraszti, J. Köhler, H. Zhang, R. Windoffer, A. Mourran, M. Möller, L. De Laporte, *Nat. Commun.* **2019**, *10*, 4027.
[52] Y. Chandorkar, C. Bastard, J. Di Russo, T. Haraszti, L. De Laporte, *Appl. Mater. Today* **2022**, *27*, 101492.
[53] A. Das, R. S. Fischer, D. Pan, C. M. Waterman, *J. Biol. Chem.* **2016**, *291*, 6096–6110.
[54] D. Missirlis, J. P. Spatz, *Biomacromolecules* **2014**, *15*, 195–205.
[55] E. E. Charrier, K. Pogoda, R. G. Wells, P. A. Janmey, *Nat. Commun.* **2018**, *9*, 449.
[56] O. Chaudhuri, J. Cooper-White, P. A. Janmey, D. J. Mooney, V. B. Shenoy, *Nature* **2020**, *584*, 535–546.

Manuscript received: July 11, 2023
Accepted manuscript online: September 15, 2023
Version of record online: September 25, 2023